Progress in Oceanography 229 (2024) 103366

Contents lists available at ScienceDirect

Progress in Oceanography

journal homepage: www.elsevier.com/locate/pocean

# Long-term variation of the eddy kinetic energy in the Northeastern South China sea

Baolan Wu [a,b,*], Jianping Gan [b,c]

[a] Advanced Institute for Marine Ecosystem Change (WPI-AIMEC), Tohoku University, Sendai, Miyagi, Japan
[b] Thrust of Earth, Ocean and Atmospheric Sciences, The Hong Kong University of Science and Technology, Guangzhou, China
[c] Center for Ocean Research in Hong Kong and Macau, Department of Ocean Science and Department of Mathematics, The Hong Kong University of Science and Technology, Hong Kong, China

ARTICLE INFO

*Keywords:*
Kuroshio
South China Sea
Long-term variation
Eddy Kinetic Energy
Baroclinic instability

ABSTRACT

The seasonal to interannual variability of eddy kinetic energy (EKE) in the Northeastern South China Sea (NE-SCS) has been widely studied and it is recognized that they are strongly related to the state of the Kuroshio pathway in the Luzon Strait. While, due to the lack of long-term observations and high-resolution simulations, the decadal change of EKE in NE-SCS remains unexplored. In this study, we show the EKE trend in the past ~ 30 years in the NE-SCS by using satellite observation and global HYbrid Coordinate Ocean Model reanalysis with the Navy Coupled Ocean Data Assimilation. It is found that due to the weakening of the Kuroshio in the Luzon Strait since 1990 s, the Kuroshio shows an enhanced looping path in the NE-SCS, inducing stronger EKE in this region. Further analysis confirms that the energy transfer by baroclinic instability is dominant for the increasing of EKE, when the Kuroshio intrudes into the NE-SCS and brings more potential energy inside the circulation. The Kuroshio state along the Luzon Strait is the key for modulating the EKE in the NE-SCS. Furthermore, the long-term weakening of Kuroshio current along the Luzon strait during 1993–2020 is determined by the decreasing of subtropical mode water, corresponding to the positive phase of the Atlantic Multidecadal Oscillation. This study provides insight into the interaction between marginal sea (i.e., the SCS) and the open ocean (i.e., the western Pacific Ocean), finally linking to the global climate change.

## 1. Introduction

In the northwestern Pacific Ocean, the largest marginal sea is South China Sea (SCS) of which average and maximum depth is over 1800 m and 5000 m, respectively (Fig. 1). The SCS, as a semi-enclosed basin, connects with the western Pacific Ocean via Luzon Strait (>2000 m), with the Sulu Sea via Mindoro Strait (<200 m), with the Java Sea via Karimata Strait (<100 m), and with the East China Sea via Taiwan Strait (<100 m). It has long been recognized that the Luzon Strait, located between Luzon and Taiwan Islands (~360 km in width), is the key and main water exchange passage linking the SCS to the western Pacific Ocean. Specifically, when the Kuroshio passes by the Luzon Strait, its intrusions could make significant contributions to the salt, heat, and momentum budgets of the SCS and therefore strongly affects the salinity, temperature, circulation, eddy generation in the Northeastern SCS (NE-SCS; e.g., Li et al., 1998; Qu et al., 2004; Nan et al., 2015; Gan et al., 2016; Sun et al., 2020) and the local climate (Qu et al., 2006; Wang Y. et al., 2006; Tozuka et al., 2015). The Kuroshio intrusions also exert strong influence on biogeochemistry and ecology in the SCS, such as nutrient distribution (Du et al., 2013), $CO_2$ fluxes (Li et al., 2020), abundance of microplastics (Liu et al., 2021) and chlorophyll-a concentration (Chang et al., 2022).

In general, the Kuroshio takes leaking, looping and leaping pathways along the Luzon Strait (Fig. 1B), corresponding to its weak and strong transports (Nan et al., 2011a; Zhang et al., 2017), and also affected by eddies (Yuan et al., 2019). Accompanied by the variability of the Kuroshio paths, particularly the Kuroshio looping pathway, the region west of Luzon Strait (i.e., NE-SCS) is one of the richest sources of mesoscale eddies within the SCS as verified by both in situ and satellite observations (Metzger and Hurlburt, 2001; Nan et al., 2011b; Sun et al., 2016). Due to their crucial roles in transporting the heat and fresh water (Chen et al., 2012; Zhang et al., 2013, 2016), regulating the upper- and deep-layer circulation (Xue et al., 2004; Zhang et al., 2013, 2016), and potentially modulating the regional climate (Qu et al., 2006; Wang et al.,

* Corresponding author.
*E-mail address:* wu.baolan.e6@tohoku.ac.jp (B. Wu).

https://doi.org/10.1016/j.pocean.2024.103366
Received 10 February 2024; Received in revised form 13 September 2024; Accepted 14 October 2024
Available online 16 October 2024

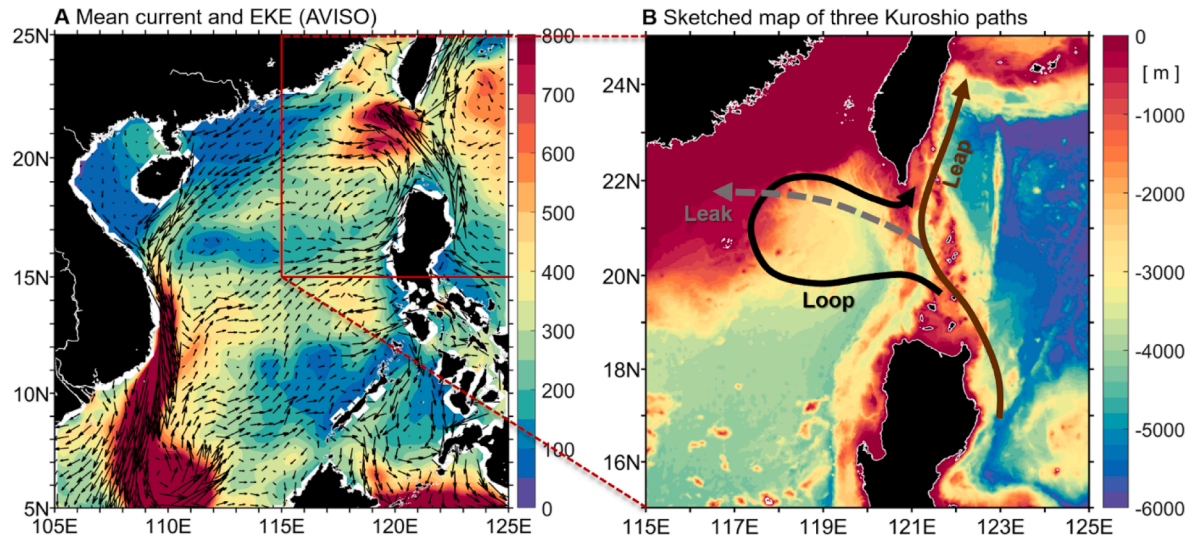


**Fig. 1.** (**A**) Spatial distribution of the winter mean (Nov.-Feb.) current (unit: m $s^{-1}$, vectors) and EKE (unit: $cm^2$ $s^{-2}$, color) derived from AVISO altimetry. Red box indicates the Northeastern South China Sea area (15°-25°N, 115°-125°E) that focused on in this study. (**B**) Sketched map of the three Kuroshio paths. The bold brown curve represents the leaping path, the bold black curve is the looping path, and the gray dashed curve is the leaking path. Color shading denotes the ocean bottom topography (unit: m) derived from the ETOPO2022 dataset.

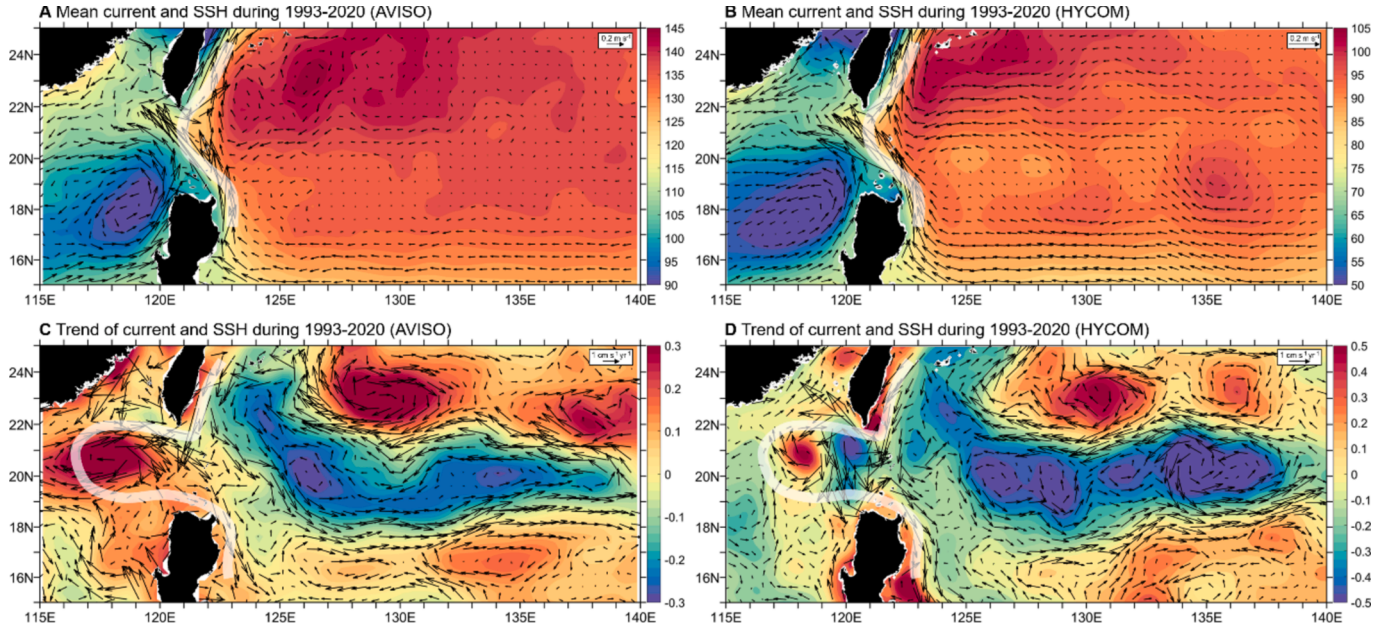


**Fig. 2.** (**A**) Spatial distribution of the winter mean (Nov.-Feb.) current (unit: m $s^{-1}$, vectors) and SSH (unit: cm, color) derived from AVISO altimetry. (**B**) Same as (**A**), but for the 0–500 m depth-averaged winter mean current and SSH from HYCOM dataset. (**C**) Linear trend of the current (unit: cm $s^{-1}$ $yr^{-1}$, vectors) and SSH (cm $yr^{-1}$, color) from 1993 to 2020 derived from AVISO altimetry. (**D**) Same as (**C**), but based on the 0–500 m depth-averaged HYCOM dataset. Notice that the global mean value of 3.2 mm $yr^{-1}$ has been subtracted out to emphasize the regional SSH trend signals. The white curve in figures indicates the sketched path of the Kuroshio current. *SSH* sea surface height.

2012), characteristics of these mesoscale eddies were widely studied in the past three decades (Hwang and Chen, 2000; Wang et al., 2003; Wang D. et al., 2008; Chen et al., 2011; Zhang et al., 2016).

The above abundant eddy activities exhibit evident imprint with high eddy kinetic energy (EKE) in the region southwest of Taiwan in the NE-SCS (Fig. 1A; Chen et al., 2009; Zhang et al., 2017). Along with geographical distribution of the EKE, its temporal variations on seasonal and interannual timescales were also investigated extensively (Chen et al., 2009; Cheng and Qi, 2010; Wang et al., 2012; Zhao et al., 2022). Besides other generation mechanisms, such as local wind (Wang G. et al., 2008) and propagation from Pacific Ocean (Zheng et al., 2011; Zheng et al., 2017), a large number of these eddies are believed to arise from variability of the Kuroshio path (Metzger and Hurlburt, 2001; Jia and Chassignet, 2011; Nan et al., 2011b). The baroclinic instability or barotropic instability associated with the Kuroshio inside the NE-SCS are the main energy source for maintain this high EKE (Zhang et al., 2017). For example, the interannual high EKE in the NE-SCS is due to the baroclinic instability with the looping path of Kuroshio (Sun et al., 2016).

While the previous studies have improved our knowledge of the eddy activities and their associated Kuroshio pathway variability, several important issues remain to be addressed. First, due to the limited

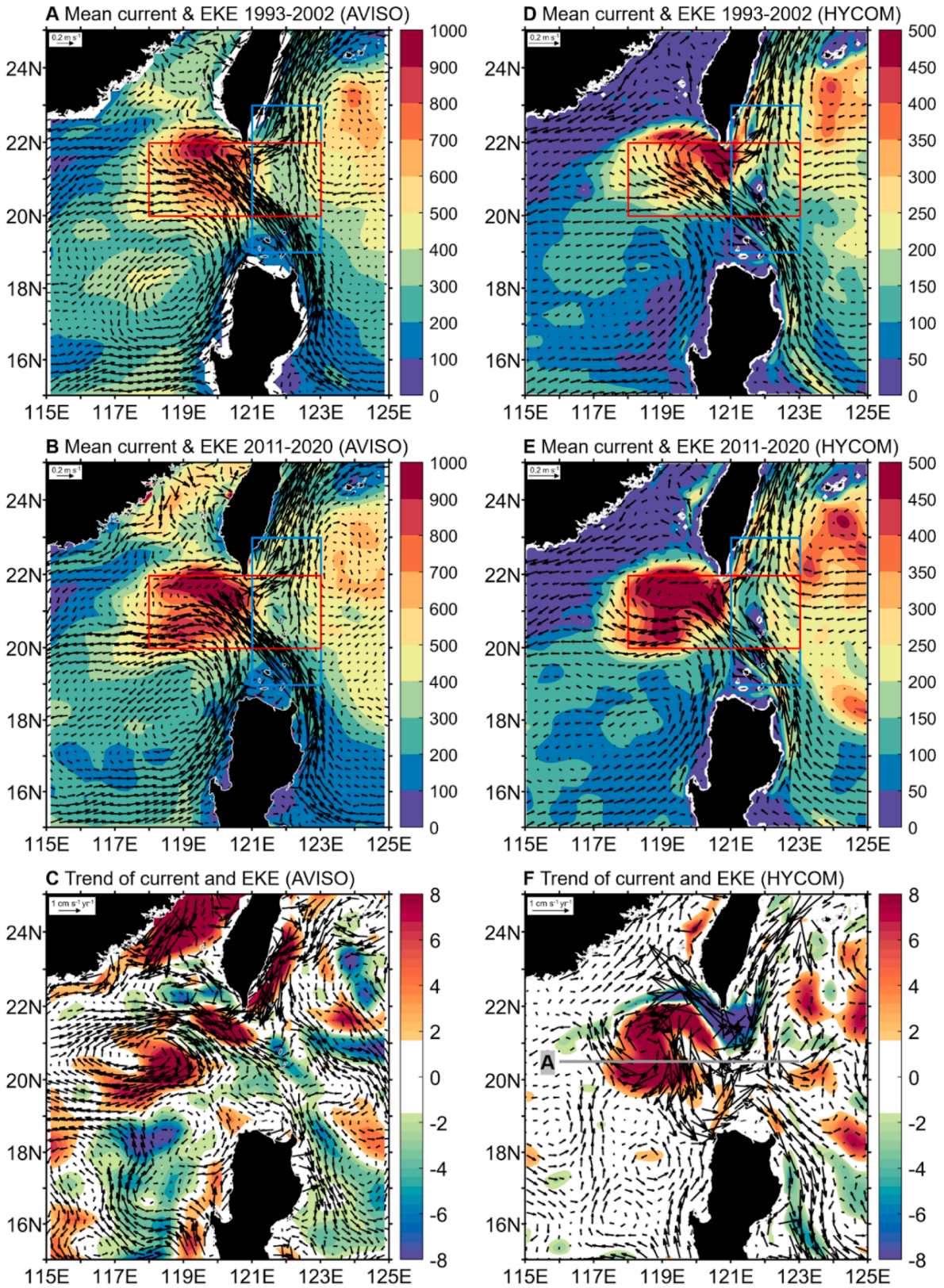


**Fig. 3.** (**A**) Spatial distribution of the winter mean (Nov.-Feb.) current (unit: m $s^{-1}$, vectors) and EKE (unit: $cm^2$ $s^{-2}$, color) during 1993–2002 derived from AVISO altimetry. (**B**) Same as (**A**), but for the period during 2011–2020. (**C**) Linear trend of the current (unit: cm $s^{-1}$ $yr^{-1}$, vectors) and EKE ($cm^2$ $s^{-2}$ $yr^{-1}$, color) from 1993 to 2020. (**D**)–(**F**) Same as (**A**)–(**C**), but based on the 0–500 m depth-averaged HYCOM dataset. Gray west-east line represents the transect A (116°-123°E, 20.5°N). Red and blue box in (**A**, **B**, **D**, **E**) indicates the area of (20°-22°N, 118°-123°E) and (19°-23°N, 121°-123°E), respectively.

observations, the long-term trend the EKE in the NE-SCS is unclear. Based on the observational and numerical data between 1993–2010, Nan et al. (2013) found that the Kuroshio looping path and eddy activities in the NE-SCS became weaker. But with longer observations (1993–2020), Wu et al. (2024) showed that the transport of Kuroshio in the Luzon Strait is weakening due to the decreasing of sea surface height along the latitudinal band of Luzon Strait, induced by the reduction of subsurface mode water volume. This in turn causes an enhanced looping path of the Kuroshio in the NE-SCS in the past 30 years, as shown in Fig. 2. Then the EKE in the NE-SCS may be increasing and this should be confirmed. Second, if the EKE is increasing, which process is dominant, barotropic instability (Zhang et al., 2017) or baroclinic instability?

To address these issues, the paper examines the long-term trend of the EKE in the NE-SCS by synergetic use of moored and satellite derived data and data-assimilative model products. The rest of this paper is organized as follows: Section 2 introduces the data, model products and related analysis methods used in this study. Section 3 presents characteristics of the Kuroshio pathway and EKE in the NE-SCS during the past 30 years. In section 4, the mechanism of EKE long-term trend is analyzed. Finally, the summary and discussion are given in section 5.

## 2. Data and methods

Two types of observational data are adopted in this study to analyze the long-term variability of EKE in the NE-SCS. As for the observational data, one is the daily satellite altimetry observations: Archiving, Validation, and Interpretation of Satellite Oceanographic data (AVISO, https://www.aviso.altimetry.fr/en/data/data-access.html). The AVISO data, with horizontal resolution of 0.25° by 0.25°, merges satellite altimetry observations from ERS-1/2, Jason-1, TOPEX/Poseidon and Envisat. Detailed information of AVISO altimetry data can be found in SSALTO/DUACS (2011). The sea level (i.e., sea surface height, SSH) is directly derived from the AVISO data and the surface geostrophic currents are computed using the horizontal gradients of SSH as follow:

$$(u_g, v_g) = \frac{g}{f}\left(-\frac{\partial SSH}{\partial y}, \frac{\partial SSH}{\partial x}\right) \tag{1}$$

where $u_g$ and $v_g$ denote the zonal and meridional geostrophic velocity, $g$ is the gravitational acceleration and $f$ is the Coriolis parameter. The EKE is estimated from $(u_g', v_g')$ by taking the departure of the mean $(u_g, v_g)$ as follow:

$$EKE = \frac{1}{2}\left(u_g'^2 + v_g'^2\right) \tag{2}$$

The other type of observational data is obtained from the objective analysis products from Institute of Atmospheric Physics (Li et al., 2023; called IAP data, https://www.ocean.iap.ac.cn/). The IAP data is monthly objective analyses of in situ observations (e.g., expendable bathy-thermographs, conductivity-temperature-depth measurements from Argo floats and research ships) with a horizontal resolution of 0.5° by 0.5°. Specifically, it provides 3-dimentional subsurface temperature and salinity data with 41 vertical levels up to 2000 m from 1960 to present. Please refer to Li et al. (2023) for more detailed information on data quality control and error estimates. In this study, we use the temperature and salinity data to characterize the water mass changes in the NE-SCS region to analyze the influence of enhanced Kuroshio looping pathway. Besides, the IAP data is also used to check the upper-layer circulation in region of NE-SCS by the thermal wind equation (i.e., a consequence of hydrostatic and geostrophic balance) as follow:

$$(u_g, v_g) = \frac{1}{\rho f}\left(-\frac{\partial P}{\partial y}, \frac{\partial P}{\partial x}\right) \tag{3}$$

where $\rho$ is the seawater density, $P$ is the pressure and the depth of 1500 m is assumed as a level of no motion according to Wu et al. (2020a).

Besides the above two types of observational data, outputs from the HYbrid Coordinate Ocean Model with Naval Research Laboratory Coupled Ocean Data Assimilation (hereafter HYCOM for brevity) are also used in this study to do the energy analysis in the region of NE-SCS. The reason we adopt the numerical simulation products from HYCOM was because it can well reproduce the sea level decreasing trend along the Luzon Strait in the western Pacific Ocean (Fig. 2), and also the enhanced Kuroshio looping pathway and the increased EKE in the NE-SCS (Fig. 3). HYCOM dataset is a daily global high-resolution simulation, with horizontal resolution of 1/12.5° by 1/12.5°. It assimilates a large number of oceanic observations (e.g., in situ temperature and salinity, as well as the satellite-based sea surface height and sea surface temperature) and can be well applied to large scale, marginal sea and coastal researches (Cummings, 2005). The thorough overview of the model configuration and optimization can be found at https://hycom.org.

According to Wu and Gan (2023), the EKE budget equation can be expressed as follow:

$$\frac{\partial EKE}{\partial t} = \overbrace{-\nabla\cdot(\vec{V}EKE)}^{①} \underbrace{-\left(\overrightarrow{V'}\cdot\nabla P'\right)}_{②} \overbrace{-\rho_0\left[u'\overrightarrow{V'}\cdot\nabla\bar{u} + v'\overrightarrow{V'}\cdot\nabla\bar{v}\right]}^{③} \underbrace{-g\rho' w'}_{④} + \overbrace{\rho_0\overrightarrow{V'}\cdot\overrightarrow{VIS'}}^{⑤} \quad (4) \tag{4}$$

where $\vec{V} = u\vec{i} + v\vec{j} + w\vec{k}$ and $\overrightarrow{VIS}$ represents the vertical viscous terms. The four terms in the right of eq (4) indicate the physical process of EKE convergence, pressure work, barotropic instability, baroclinic instability and vertical viscosity, respectively. The baroclinic and barotropic instabilities of the mean current primarily contribute to the energy of mesoscale eddies (Pedlosky, 1987). The baroclinic instability term (BC term) and barotropic instability term (BT term) in the EKE budget equation are the major eddy energy sources in the region of NE-SCS, revealing by the previous studies (e.g., Yang et al., 2013; Zhang et al., 2013; Zu et al., 2013; Sun et al., 2016). Specifically, the BC term and BT term can be quantified at each grid point as follow:

$$\text{BC term} = -g\rho' w' \tag{5}$$

$$\text{BT term} = -\rho_0 \boldsymbol{V_h}' \bullet (\boldsymbol{V_h}' \bullet \nabla\overline{\boldsymbol{V_h}}) = -\rho_0\left(u'^2\frac{\partial\bar{u}}{\partial x} + v'^2\frac{\partial\bar{v}}{\partial y} + u'v'\frac{\partial\bar{u}}{\partial y} + u'v'\frac{\partial\bar{v}}{\partial x}\right) \tag{6}$$

where $w$ is the vertical velocity, $\boldsymbol{V_h} = (u, v)$ is the horizonal velocity vector and $\rho_0 = 1025$ kg m$^{-3}$ derived from HYCOM output.

Here, we focus on the Kuroshio looping pathway induced EKE and its long-term variation in the NE-SCS during 1993–2020. Because the Kuroshio looping current primarily occurs in winter (Wang and Chern, 1987; Wu and Chiang, 2007; Jia and Chassignet, 2011; Nan et al., 2015; Zhang et al., 2017), all the variables are winter-mean results (the winter

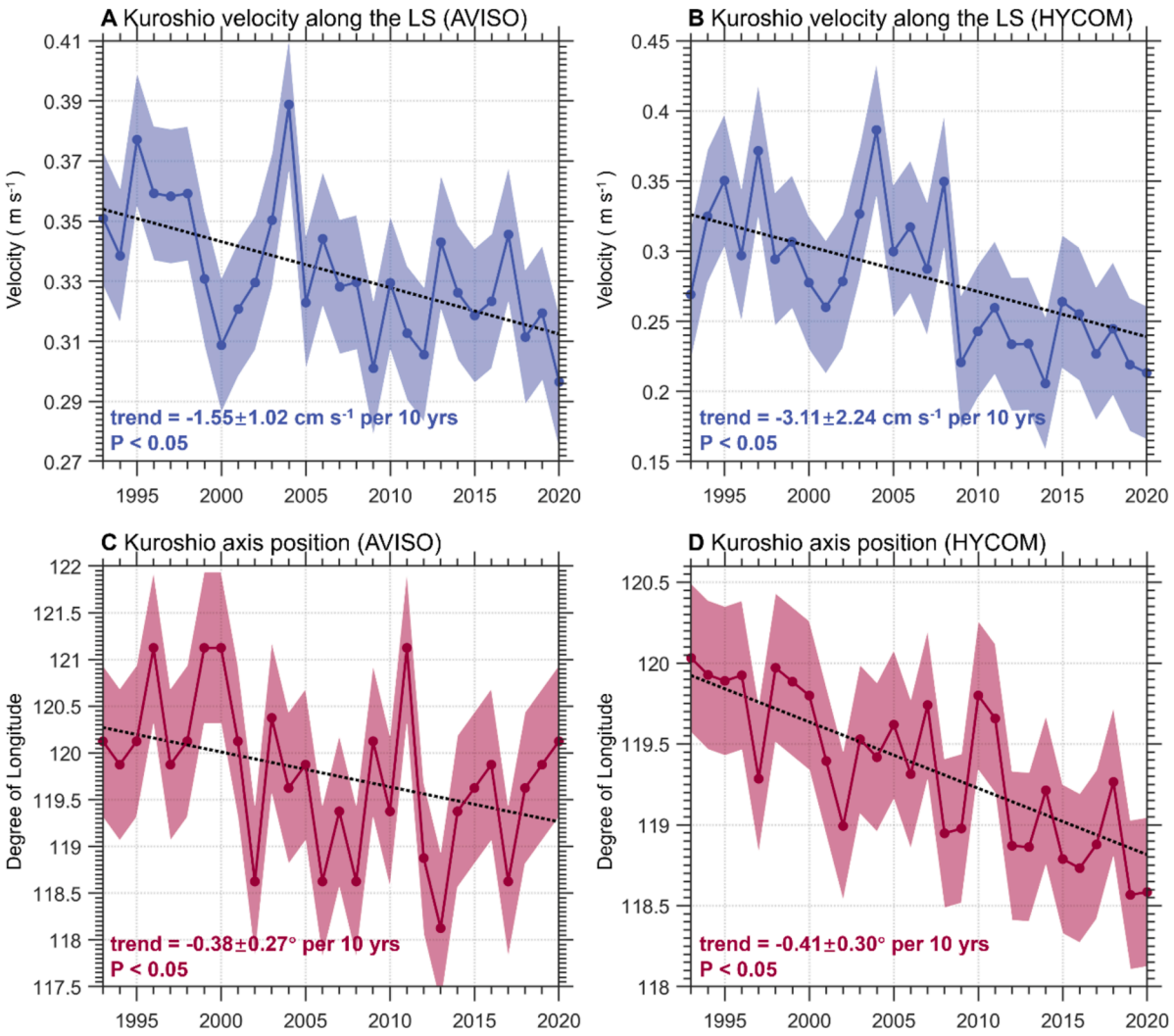


**Fig. 4.** (A) Kuroshio velocity (unit: m $s^{-1}$) averaged in the region of 19°–23°N, 121°-123°E along the LS derived from AVISO altimetry. (B) Same as (A), but based on the 0–500 m depth-averaged HYCOM dataset. (C) Kuroshio axis position (unit: degree of longitude) averaged in the region of 20°–22°N, 118°-123°E derived from AVISO altimetry. (D) Same as (C), but based on the 0–500 m depth-averaged HYCOM dataset. The shadings for each line show the one standard deviations of their time series. P value smaller than 0.05 indicates that the trend is significant at the 5 % significance level. Note that the Fig. 4A and 4C are modified from the Fig. 2B and 2D in Wu et al., (2024). LS Luzon strait.

is defined as November-February hereafter) in this study. Besides, according to the previous studies (e.g., Zhang et al., 2015; Sun et al., 2016), the depth of 500 m can be regarded as the interface between the upper and intermediate layers of the SCS circulation with HYCOM EKE showing little signals below. Hence, the variables from HYCOM and IAP dataset are 500 m-averaged value in this study without specifications. The 5 % significance level is used for all statistical analysis in this study following Bretherton et al. (1999).

## 3. Enhanced Kuroshio looping path and related EKE trend

Both observation (Fig. 2A) and numerical model (Fig. 2B) show that the Kuroshio is passing by the Luzon Strait with a climatology bending structure, and its path varies with the Kuroshio transport (Nan et al., 2011a). The recent study by Wu et al. (2024) demonstrates that the sea level along the latitudinal band of Luzon Strait shows significant decrease during 1993–2020 (Fig. 2C and 2D), induced by the reduction of subsurface mode water volume. Correspondingly, this sea level decreasing along the Luzon Strait results in a weakened Kuroshio current and enhanced looping path in the NE-SCS, as shown in the AVISO observational (Fig. 2C) and HYCOM data (Fig. 2D). The region with enhanced Kuroshio looping path coincides with the region of prominent positive SSH anomalies (Fig. 2C and 2D), indicating clockwise eddy activities. Such kind of structure will change the EKE in the NE-SCS and the detailed features are presented as follows.

To further illustrate the relation between the Kuroshio path and EKE changes during 1993–2020, we examine two decadal-averaged state of current and EKE in the NE-SCS by comparing 1993–2002 (first 10 years) and 2011–2020 (last 10 years) periods. From the AVISO observation, it can be readily seen that the Kuroshio is stronger in the first 10-year period than that in the last 10-year period as indicated by the current vectors in Fig. 3A and 3B. Along with the weakened Kuroshio and intensified anticyclonic loop, the EKE exhibits larger value in the second period in the NE-SCS as indicated by the color shading in Fig. 3A and 3B. This is more clearly when we look at the trend of current and EKE from 1993 to 2020 as shown in Fig. 3C: southward trend of the current against the mean northward current along the Luzon Strait results in decreased Kuroshio velocity and enhanced looping path with increasing EKE trend in the NE-SCS. The EKE increases at a rate of ~ 80 cm2 s-2 per decade from 1993 to 2020 (color shading in Fig. 3C). The spatial distribution of the current and EKE trend from HYCOM dataset is consistent with that from AVISO observations (Fig. 3D-3F). Note that the value of current and EKE from HYCOM dataset (Fig. 3D and 3E) is smaller than that from AVISO observations (Fig. 3A and 3B), because the former is 0–500 m

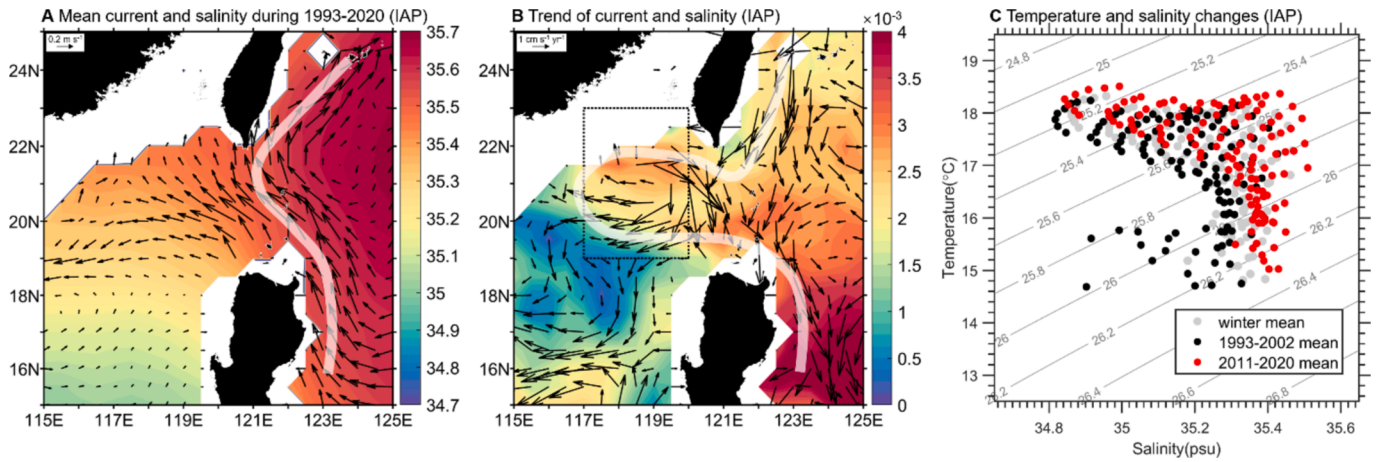


**Fig. 5.** (**A**) Spatial distribution of the winter mean (Nov.-Feb.) current (unit: m $s^{-1}$, vectors) and salinity (unit: psu, color) derived from the 0–500 m depth-averaged IAP dataset. (**B**) Linear trend of the current (unit: cm $s^{-1}$ $yr^{-1}$, vectors) and salinity (psu $yr^{-1}$, color) from 1993 to 2020. The white curve in figures indicates the sketched path of the Kuroshio current. Black dashed box indicates the main area of the Kuroshio looping path (19°–23°N, 117°-120°E). (**C**) T-S diagram of the 0–500 m depth-averaged water mass in the region of 19°–23°N, 117°-120°E (black dashed box in figure B). Gray dots are the winter-mean water mass during 1993–2020, black dots are for the winter mean during 1993–2002 and red dots are for the winter mean during 2011–2020.

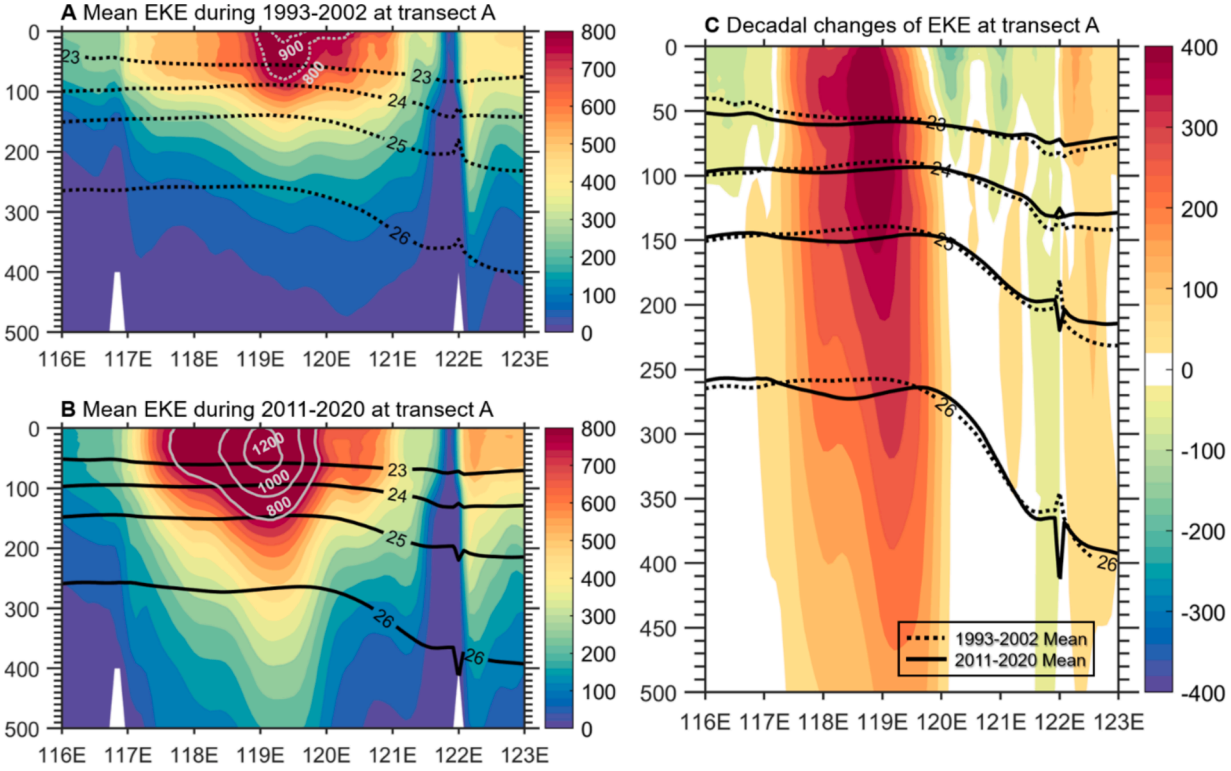


**Fig. 6.** (**A**) Mean EKE (unit: $cm^2$ $s^{-2}$, color) and density (unit: kg $m^{-3}$, black contours) in winter (Nov.-Feb.) during 1993–2002 at transect A along 20.5°N, based on the HYCOM dataset. Gray contour denotes the EKE value of 800 $cm^2$ $s^{-2}$ and 900 $cm^2$ $s^{-2}$ as indicated. (**B**) Same as (A), but for the period during 2011–2020. Gray contour denotes the EKE value of 800 $cm^2$ $s^{-2}$, 1000 $cm^2$ $s^{-2}$ and 1200 $cm^2$ $s^{-2}$ as indicated. (**C**) Decadal changes of EKE between 1993–2002 and 2011–2020 (latter minus former, unit: $cm^2$ $s^{-2}$, color) at transect A along 20.5°N. The dashed and solid contours indicate the winter-mean (Nov.-Feb.) isopycnals during 1993–2002 and 2011–2020, respectively.

depth-averaged results. But the trend of EKE is similar (Fig. 3C and 3F) for both datasets, indicating the trend is robust not only in the surface but also to the subsurface ocean.

Besides the spatial pattern of the current and EKE trend during 1993–2020, the region-averaged time series of the Kuroshio velocity and its axis position are also conducted as the index of Kuroshio strength and pathway. As for the Kuroshio velocity along the Luzon Strait that averaged in the region of 19°–23°N, 121°-123°E, it shows a decreasing trend of ~ -1.55 ± 1.02 cm $s^{-1}$ per decade with AVISO altimetry (Fig. 4A) and ~ -3.11 ± 2.24 cm $s^{-1}$ per decade (Fig. 4B) with HYCOM dataset. This is consistent with the weakening of the Kuroshio as shown in Fig. 3. For the Kuroshio axis position defined as the location of the maximum meridional velocity within the region of 20°–22°N, 118°-123°E, it shifts westward at a rate of ~ -0.38 ± 0.27° per decade (Fig. 4C) and ~ -0.41 ± 0.30° per decade (Fig. 4D) derived from AVISO altimetry and HYCOM dataset, respectively. The westward shift of the

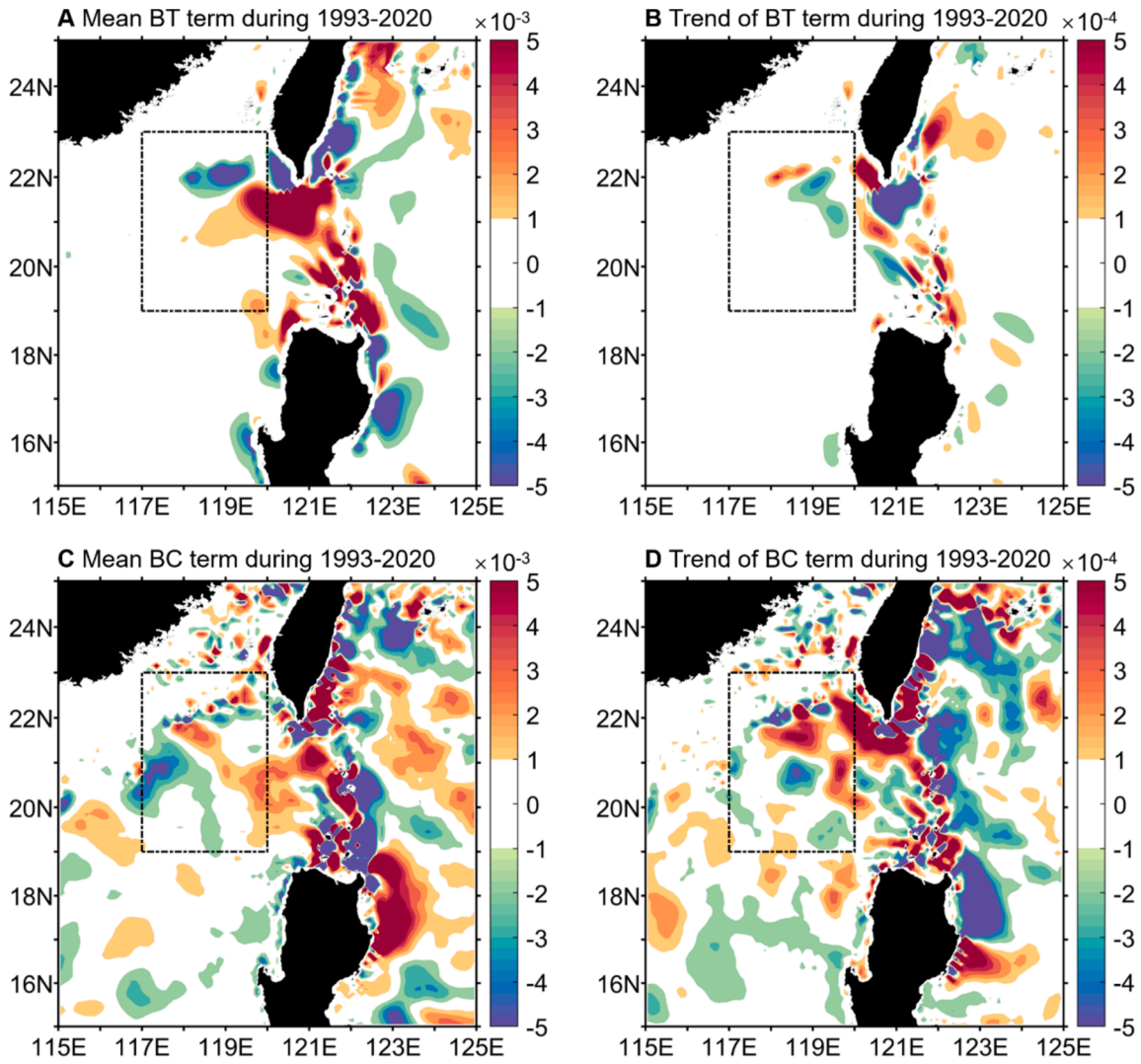


**Fig. 7.** (**A**) Spatial distribution of the 0–500 m depth-integrated winter-mean (Nov.-Feb.) BT term (unit: W $m^{-3}$, color) based on the HYCOM dataset. (**B**) Trend of the BT term (unit: W $m^{-3}$ $yr^{-1}$, color) during 1993–2020. Black dashed box indicates the main area of the Kuroshio looping path (19°–23°N, 117°-120°E). (**C**) and (**D**) Same as (**A**) and (**B**), but for the BC term.

Kuroshio axis also confirms the looping path of the Kuroshio in the NE-SCS.

Coincide with the Kuroshio enhanced looping path, the properties of sea water in the NE-SCS would be influenced since the water mass of Kuroshio and SCS are different. To examine the change of water mass properties in the NE-SCS during 1993–2020, the three-dimensional subsurface temperature and salinity from IAP data is utilized (Fig. 5). On the one hand, the mean current calculated by the thermal wind equation (see Data and Methods) averaged in the upper 500 m from IAP data well shows the basic circulation around the Luzon Strait region with intensified western boundary currents (Fig. 5A). The trend of current exhibits obvious anticyclonic loop during the period of 1993–2020 (Fig. 5B), which is consistent with the pattern from AVISO altimetry and HYCOM dataset (Fig. 3C and 3F). On the other hand, the enhanced looping path of the Kuroshio in recent years changes the properties of water mass in the NE-SCS, by bring more upper-layer Kuroshio water from western Pacific Ocean into the NE-SCS. We should note that the Kuroshio water is warmer and salter than that in the NE-SCS. The enhanced Kuroshio intrusion can be readily seen in the T-S diagram of the 0–500 m depth-averaged water mass in the region of 19°–23°N, 117°-120°E (Fig. 5B and 5C), with the water temperature and salinity increasing in the last 10-year period (red dots in Fig. 5C) than that in the first 10-year period (black dots in Fig. 5C).

Through the above analysis, it is confirmed that the Kuroshio experienced an enhanced looping path in the past ~ 30 years. The larger anticyclonic loop brings warmer and salter water into the upper-layer NE-SCS, forming a strong oceanic front and velocity shears. Coincide with these processes, an increasing trend of EKE in the region of NE-SCS during 1993–2020 was revealed. The detailed mechanism is further investigated in the following section.

## 4. Mechanism

To better understand the dynamics of long-term increasing trend of the EKE in the NE-SCS, zonal sections of EKE (color shading) and density (contours) were constructed at transect A along 20.5°N (gray line in Fig. 3F) for the two periods, 1993–2002 and 2011–2020, respectively (Fig. 6A and 6B). Obviously, the EKE mainly concentrate in the upper 500 m and its value is much larger in the second period (maximum > 1200 $cm^2$ $s^{-2}$) than that in the first period (maximum > 900 $cm^2$ $s^{-2}$), with the maximum EKE shifting westward from 119.5°E to 118.5°E. The differences in the surface-to-subsurface EKE between the two periods (1993–2002 and 2011–2020, latter minus former) can be generally regarded as its long-term trend in the past 30 years. We can find that the intensification of EKE (color shading in Fig. 6C) has occurred both at the surface and in the subsurface layers around the longitude of 118.5°E,

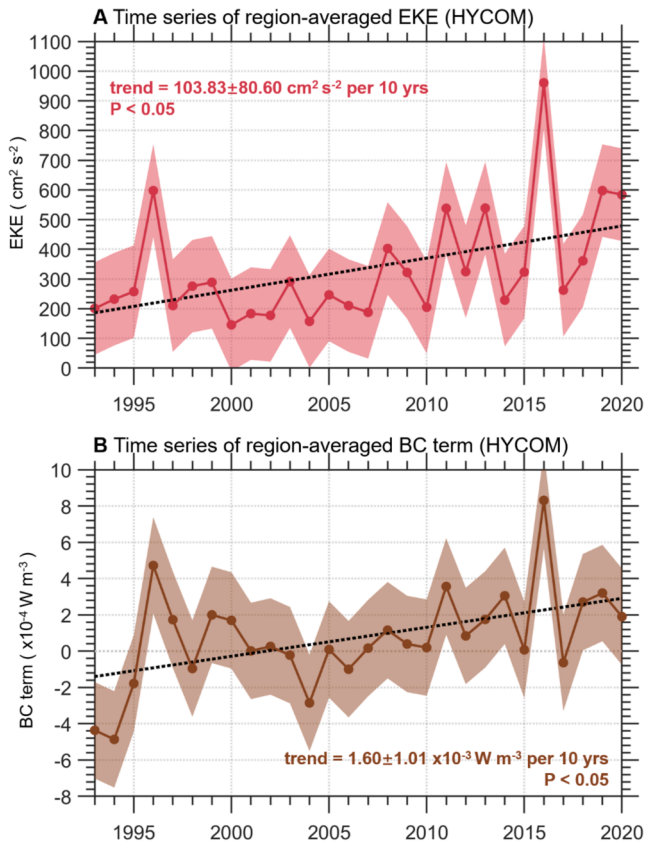


**Fig. 8.** (**A**) Time series of the 0–500 m depth-averaged winter-mean (Nov.-Feb.) EKE (unit: $cm^2\ s^{-2}$) from HYCOM dataset, averaged in the main area of the Kuroshio looping path (19°–23°N, 117°-120°E). (**B**) Time series of the 0–500 m depth-integrated winter-mean (Nov.-Feb.) BC term (unit: $W\ m^{-3}$) from HYCOM dataset, averaged in the main area of the Kuroshio looping path (19°–23°N, 117°-120°E). The shadings for each line show the one standard deviations of their time series. P value smaller than 0.05 indicates that the trend is significant at the 5 % significance level.

where is the core of the Kuroshio enhanced anticyclonic looping pathway (Fig. 3). Along with the increasing of EKE, the thermocline demonstrates a "U" structure change in the maximum EKE region corresponding to the enhanced looping path of the Kuroshio, indicating a strong potential energy source (Fig. 6C).

So far, the enhanced looping path of the Kuroshio results in the long-term increasing of EKE could be explained by two dynamical processes: one is the horizontal velocity shear (i.e., barotropic instability) presented by the anticyclonic loop current (Fig. 3), and the other is the vertical velocity shear (i.e., baroclinic instability) presented by the density front within the Kuroshio loop current (Fig. 6). This is consistent with previous studies that the baroclinic instability and barotropic instability are the major EKE sources in the region of NE-SCS (Yang et al., 2013). For example, Zhang et al. (2013) find that the eddy pairs in the NE-SCS are generated by the barotropic instability. While Sun et al. (2016) highlight the importance of baroclinic instability in determining the interannual variability of EKE in the NE-SCS. For the long-term increasing trend of EKE in the NE-SCS, which process is dominant will be further checked by the EKE budget in the following analysis.

Quantificationally, the two major source terms were calculated by using the HYCOM outputs, the BT term (i.e., barotropic instability) and the BC term (i.e., baroclinic instability) to evaluate their contributions on the long-term increasing trend of EKE in the NE-SCS region. The mean BT term is large along the Kuroshio current where the horizontal velocity shear is strong (Fig. 7A). The spatial pattern of BT trend during 1993–2020 is patchy and mainly confined in the Luzon Strait with much weaker signals in the NE-SCS (Fig. 7B). In terms of the BC term, its mean amplitude strengthens from the open Ocean westward to the Luzon Strait and also the NE-SCS region (Fig. 7C), indicating the BC term is more dominant that the BT term in the NE-SCS. This is further confirmed by the trend of BC term during 1993–2020 (Fig. 7D). The BC term increases in the broad area in the NE-SCS and the large BC trend is near the maximum EKE increasing region (also the core looping path of the Kuroshio). Although the spatial pattern of BC term trend also looks patchy in the whole basin, its positive trend value is dominate in the region of 19°-23°N, 117°-120°E. The trend of the BC term displays a positive value in the NE-SCS with the maximum rate around $4 \times 10^{-3}$ W $m^{-3}$ per decade.

More specifically, we compared the time series of area-averaged EKE (Fig. 8A) and BC term (Fig. 8B) in the core region of the Kuroshio looping path (19°–23°N, 117°-120°E) in the upper 500 m. It is shown that the region-averaged EKE has increased at a rate of $\sim 103.83 \pm 80.6$ $cm^2\ s^{-2}$ per decade (Fig. 8A) and the BC term correspondingly increases at a rate of $\sim 1.60 \pm 1.01 \times 10^{-3}$ W $m^{-3}$ per decade (Fig. 8B). Notice that the BC term and EKE changes consistently on not only long-term trend time scale, but also on the interannual time scale which was revealed by Sun et al. (2016). Correlation coefficient between the region-averaged EKE and BC term at zero lag is 0.82, that is statistically significant above the 95 % confidence level. This further confirms the dominant role for BC term in the change of EKE long-term variation in the NE-SCS during 1993–2020.

Note that the local wind forcing may also play an important role in the eddy generations in the NE-SCS as proposed by previous studies (e.g., Wang G. et al., 2008). However, Sun et al. (2016) pointed out that the interannual variation of the local wind stress curl rarely influences the EKE southwest of Taiwan. Besides, the recent studies found that the subtropical atmospheric circulation (Zhou et al., 2024) and its curl (Zhang et al., 2020) has been weakened under the recent global warming. That is to say, the wind forcing seems not to explain the long-term increasing trend of EKE in the NE-SCS region and further studies are needed in the future. To summarize, the increasing trend of EKE in the NE-SCS during the past ~ 30 years is primarily induced by the enhanced Kuroshio looping pathway. The mechanism is understood as below: when the Kuroshio is weakened, the Kuroshio looping path gets enhanced, vertical shear of velocity becomes increased west of the Luzon Strait, which intensifies baroclinic instability of the current, and finally leads to an increasing trend of EKE in the NE-SCS.

## 5. Discussion and conclusion

In this study, the EKE trend in the past 30 years in the NE-SCS is examined by using AVISO observation and HYCOM assimilation data. It is found that due to the weakening of the Kuroshio along the Luzon Strait since 1990 s, the Kuroshio shows an enhanced looping path in the NE-SCS, inducing stronger EKE in this region. Analysis confirms that the energy transfer by baroclinic instability is dominant for the increasing of EKE, when the Kuroshio intrudes into the NE-SCS and brings more potential inside the circulation. In addition, the southern part of the enhanced energy EKE center west of Luzon Strait is related the to the Luzon cold eddy (e.g., Shaw, 1996; Yang and Liu, 2003), which can be further seen in Figs. 9A and 9B as indicated by the blue contours. When the Kuroshio weakens with enhanced looping path as shown in Fig. 9B in the last 10 years (2011–2020), the Luzon cold eddy moves further northwestward comparing with that in the first 10 years (1993–2002, Fig. 9A). Then, there is a stronger SSH gradient between the Luzon cold eddy (blue contours) and the Kuroshio (red contours) in the northeastern SCS (Figs. 9C and 9D). The above conditions favor the instability process, which finally induces higher EKE around the region of 20°N.

Although weakening of the Kuroshio can be induced by many reasons such as North Equatorial Current migration and bifurcation and reduction of subtropical mode waters (e.g., Wu et al., 2024), it is clear that the circulation and EKE in the SCS could not only be determined by

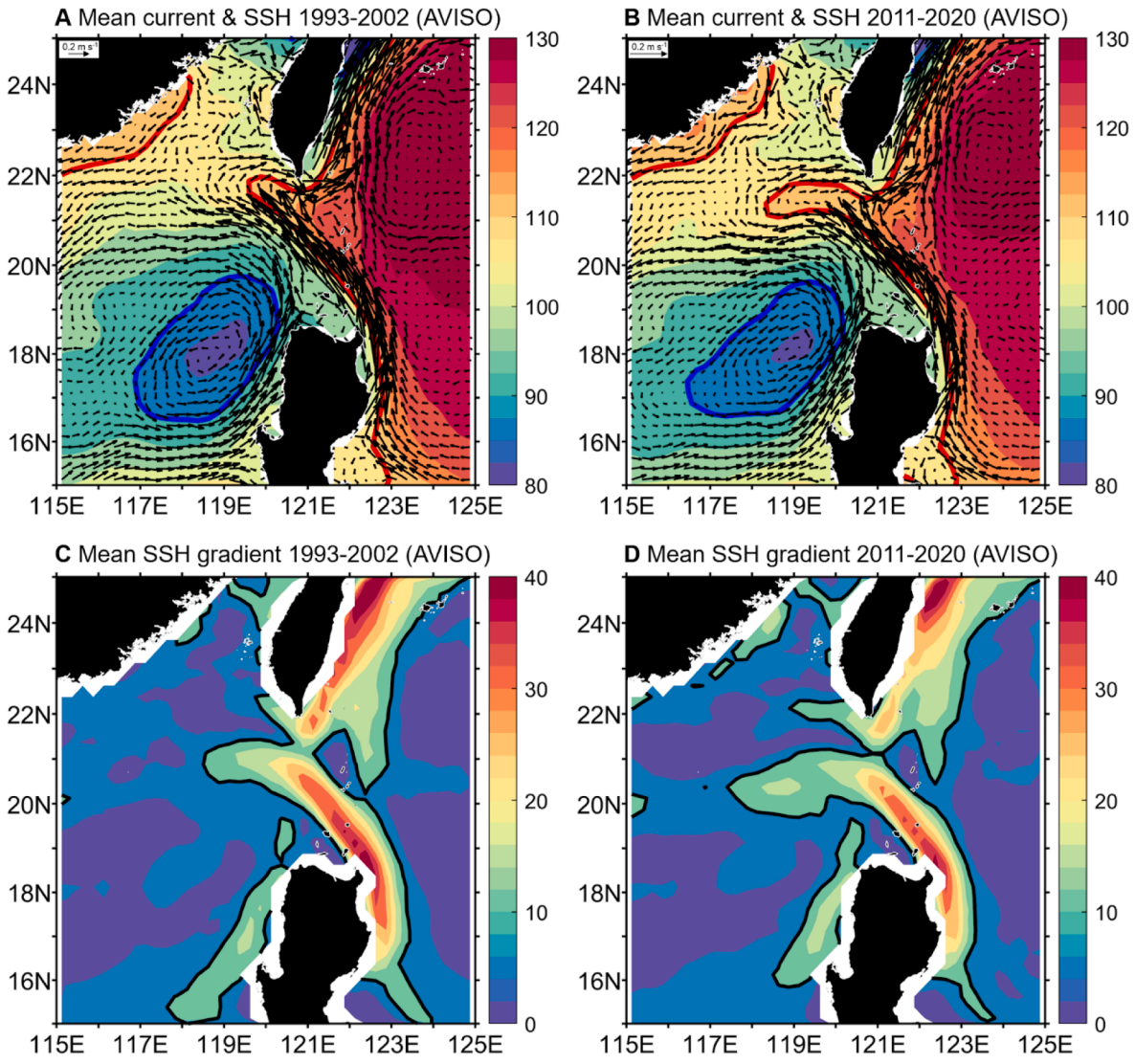


**Fig. 9.** (**A**) Spatial distribution of the winter mean (Nov.-Feb.) current (unit: m $s^{-1}$, vectors) and SSH (unit: cm, color) during 1993–2002 derived from AVISO altimetry. (**B**) Same as (**A**), but for the period during 2011–2020. Red and blue contours indicate 110-cm and 90-cm SSH contour, respectively. Here, the 110-cm SSH isoline is adopted to characterize the Kuroshio axis. (**C**) Spatial distribution of the winter mean (Nov.-Feb.) SSH horizontal gradient [unit: cm $(100\ km)^{-1}$] during 1993–2002 derived from AVISO altimetry. Black contours indicate 10 cm $(100\ km)^{-1}$ SSH horizontal gradient. (**D**) Same as (**C**), but for the period during 2011–2020.

the local forcing but also modulated by the remote forcing from the open Ocean. Especially, the open Ocean forcing can propagate by the Rossby wave along the same latitude or by the mode water from other latitudes (Fig. 10). Furthermore, it seems that the high EKE anomalies in the NE-SCS could propagate southwestward along the continental shelf (indicated by the grey contours in Fig. 10A) and even reach to the southern SCS. Thus, here comes the question: how does this EKE signal interact with the circulation and affect the environment in the entire SCS? This will be addressed in the future study.

The Kuroshio state along the Luzon Strait is the key for modulating the EKE in the NE-SCS. In terms of the dynamics on the Kuroshio state variation along the Luzon Strait (leaking or the Luzon Strait transport, LST, looping with week transport and leaping with strong transport), previous studies have investigated the relationship between the Kuroshio path and its strength (e.g., Nan et al., 2015). It is found that the Kuroshio intrusion (i.e., LST) decreased in the past two decades, both in the upper (Nan et al., 2013) and bottom layers (Zhu et al., 2022). They attribute the decreased LST to the enhanced Kuroshio transport in the east of Luzon, when the southward migration of the North Equatorial Current bifurcation responses to wind changes by Pacific Decadal Oscillation in the past two decades (Nan et al., 2015; Wu et al., 2017), which will further make the Kuroshio to bypass the Luzon Strait with leaping path (Nan et al., 2011a; 2013; Wu et al., 2016).

However, the results in this study demonstrate that the LST is not directly related to the strength of Kuroshio near Luzon Strait, i.e., not as simple as strong Kuroshio in the east of Luzon inducing weakened LST. For example, here we show the Kuroshio weakens along Luzon and Luzon Strait in the recent two to three decades, as shown in Fig. 2, while the observed LST also weakens (Zhu et al., 2022). Moreover, if Luzon Strait is the only passage with no other straits linking the South China Sea with the surrounding Oceanic basins, there will be no net LST although the Kuroshio path in the Luzon Strait still has different patterns with varying Kuroshio transport or eddy activities (Sheremet, 2001; Yuan and Wang, 2011). The opening of other straits is the key for setting up the LST, which can be explained by the 'Island Rule' (Wang D. et al., 2006; Wang Y. et al., 2006).

Besides the local forcing, the Kuroshio state near the Luzon Strait could also be affected by subsurface signal from remote forcing. The recent study confirms that the long-term weakening of Kuroshio current in the Luzon Strait in the past 30 years is due to the decreasing of sea level along the Luzon Strait latitudinal band, which is caused by the reduction of subtropical mode water (Wu et al., 2024), corresponding to

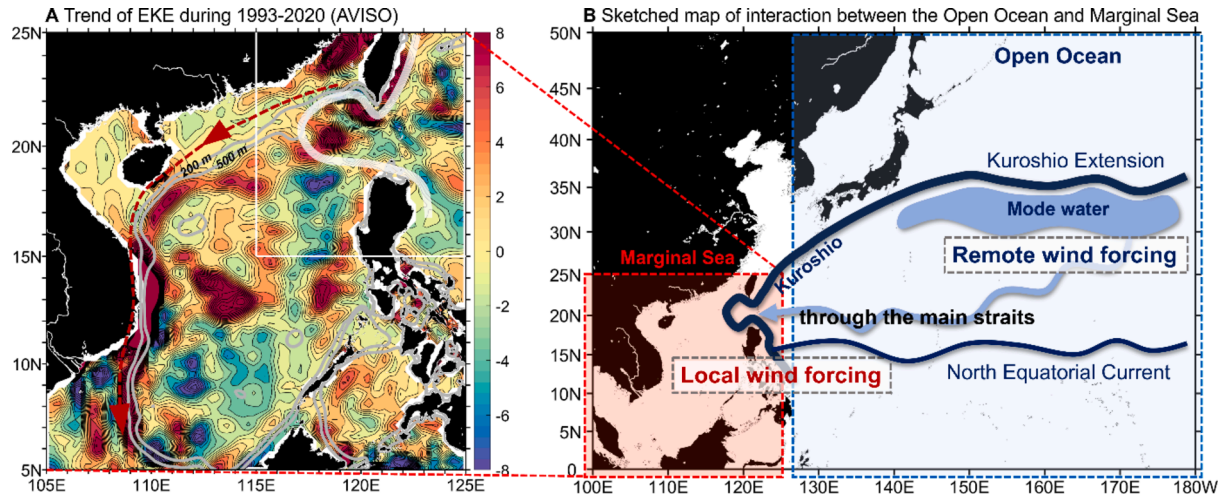


**Fig. 10.** (**A**) Spatial distribution of the linear trend of EKE ($cm^2\ s^{-2}\ yr^{-1}$, color and black contours) in winter (Nov.-Feb.) from 1993 to 2020 derived from AVISO altimetry. Red dashed line with arrow indicates the potential propagation pathway of the EKE anomalies along the continental shelf from the Luzon Strait. Gray contours represent the isobath of 200 m and 500 m. White box indicates the Northeastern South China Sea area (15°-25°N, 115°-125°E) that focused on in this study. The white curve indicates the sketched looping path of the Kuroshio current. (**B**) Sketched map of interaction between the Open Ocean (i.e., the western North Pacific Ocean) and Marginal Sea (i.e., South China Sea).

the positive phase of the Atlantic Multidecadal Oscillation (Wu et al., 2020b, 2022; Wu and Xu, 2023). That is to say, the circulation and EKE in the SCS are not only determined by the local forcing but also modulated by the remote forcing from the open Ocean. Especially, the open Ocean forcing can propagate by the Rossby wave along the same latitude or by the mode water from other latitudes (Fig. 9B). Further studies are needed to explore the dynamics of the circulation in the Western Pacific and its impact on the South China Sea.

## CRediT authorship contribution statement

**Baolan Wu:** Writing – original draft, Visualization, Validation, Project administration, Methodology, Funding acquisition, Formal analysis, Data curation, Conceptualization. **Jianping Gan:** Writing – review & editing, Supervision, Project administration, Funding acquisition, Conceptualization.

## Declaration of competing interest

The authors declare that they have no known competing financial interests or personal relationships that could have appeared to influence the work reported in this paper.

## Acknowledgments

This study is supported by the National Natural Science Foundation of China92058203 to Baolan Wu and (41930539) to Jianping Gan. This study benefited from discussions with Zhongya Cai about the coding details.

## Data availability

Data will be made available on request.

## References

Bretherton, C.S., Widmann, M., Dymnidov, V.P., Wallace, J.M., Blade, I., 1999. The effective number of spatial degrees of freedom of a time-varying field. J. Clim. 12, 1990–2009. https://doi.org/10.1175/1520-0442(1999)012<1990:TENOSD>2.0.CO;2.

Chang, Y., et al., 2022. Decreasing trend of Kuroshio intrusion and its effect on the chlorophyll-a concentration in the Luzon Strait, South China Sea. Giscience & Remote Sensing 59 (1), 633–647. https://doi.org/10.1080/15481603.2022.2051384.

Chen, G., Hou, Y., Chu, X., Qi, P., 2009. The variability of eddy kinetic energy in the South China Sea deduced from satellite altimeter data. Chin. J. Oceanol. Limnol. 27 (4), 943–954. https://doi.org/10.1007/s00343009-9297-6.

Chen, G., Hou, Y., Chu, X., 2011. Mesoscale eddies in the South China Sea: Mean properties, spatiotemporal variability, and impact on thermohaline structure. J. Geophys. Res. 116, C06018. https://doi.org/10.1029/2011JD016244.

Chen, G., Gan, J., Xie, Q., Chu, X., Wang, D., Hou, Y., 2012. Eddy heat and salt transports in the South China Sea and their seasonal modulations. J. Geophys. Res. 117, C05021. https://doi.org/10.1029/2011JC007724.

Cheng, X., Qi, Y., 2010. Variations of eddy kinetic energy in the South China Sea. J. Oceanogr. 66 (1), 85–94. https://doi.org/10.1007/s108 72-010-0007-y.

Cummings, J.A., 2005. Operational multivariate ocean data assimilation. Quart. J. Royal Met. Soc. 131 (613), 3583–3604. https://doi.org/10.1256/qj.05.105.

Du, C., Liu, Z., Dai, M., Kao, S.-J., Cao, Z., Zhang, Y., Huang, T., Wang, L., Li, Y., 2013. Impact of the Kuroshio intrusion on the nutrient inventory in the upper northern South China Sea: insights from an isopycnal mixing model. Biogeosciences 10, 6419–6432. https://doi.org/10.5194/bg-10-6419-2013.

Gan, J., Liu, Z., Hui, C., 2016. A three-layer alternating spinning circulation in the South China Sea. J. Phys. Oceanogr. 46, 2309–2315. https://doi.org/10.1175/JPO-D-16-0044.1.

Hwang, C., Chen, S.-A., 2000. Circulations and eddies over the South China Sea derived from TOPEX/Poseidon altimetry. J. Geophys. Res. 105 (C10), 23943–23965. https://doi.org/10.1029/2000JC900092.

Jia, Y., Chassignet, E.P., 2011. Seasonal variation of eddy shedding from the Kuroshio intrusion in the Luzon Strait. J. Oceanogr. 67, 601–611. https://doi.org/10.1007/s10872-011-0060-1.

Li, G., et al., 2023. A global gridded ocean salinity dataset with 0.5° horizontal resolution since 1960 for the upper 2000 m. Front. Mar. Sci. 10. https://doi.org/10.3389/fmars.2023.1108919.

Li, Q., Guo, X., Zhai, W., Xu, Y., Dai, M., 2020. Partial pressure of CO2 and air-sea CO2 fluxes in the South China Sea: Synthesis of an 18-year dataset. Prog. Oceanogr. https://doi.org/10.1016/j.pocean.2020.102272.

Li, L., Nowlin Jr, W.D., Jilan, S., 1998. Anticyclonic rings from the Kuroshio in the South China Sea. Deep Sea Res. Part I 45 (9), 1469–1482. https://doi.org/10.1016/S0967-0637(98)00026-0.

Liu, M., et al., 2021. Microplastics in the western Pacific and South China Sea: Spatial variations reveal the impact of Kuroshio intrusion. Environ. Pollut. 288, 117745. https://doi.org/10.1016/j.envpol.2021.117745.

Metzger, E.J., Hurlburt, H.E., 2001. The nondeterministic nature of Kuroshio penetration and eddy shedding in the South China Sea. J. Phys. Oceanogr. 31, 1712–1732. https://doi.org/10.1175/1520-0485(2001)031<1712:TNNOKP>2.0.CO;2.

Nan, F., Xue, H., Chai, F., Shi, L., Shi, M., Guo, P., 2011a. Identification of different types of Kuroshio intrusion into the South China Sea. Ocean Dyn. 61, 1291–1304. https://doi.org/10.1007/s10236-011-0426-3.

Nan, F., Xiu, P., Chai, F., Shi, M., Guo, P., 2011b. Oceanic eddy formation and propagation southwest of Taiwan. J. Geophys. Res. 116, C12045. https://doi.org/10.1029/2011JC007386.

Nan, F., Xue, H., Chai, F., Wang, D., Yu, F., Shi, M., Guo, P., Xiu, P., 2013. Weakening of the Kuroshio Intrusion into the South China Sea over the Past Two Decades. J. Climate 26, 8097–8110. https://doi.org/10.1175/JCLI-D-12-00315.1.

Nan, F., Xue, H., Yu, F., 2015. Kuroshio intrusion into the South China Sea: A review. Prog. Oceanogr. 137 (A), 314–333. https://doi.org/10.1016/j.pocean.2014.05.012.

Pedlosky, J., 1987. Geophysical Fluid Dynamics, 2nd ed., 710 pp.,. Springer, N. Y.
Qu, T., Du, Y., Sasaki, H., 2006. South China Sea throughflow: A heat and fresh- water conveyor. Geophys. Res. Lett. 33, L23617. https://doi.org/10.1029/2006GL028350.
Qu, T.D., Kim, Y.Y., Yaremchuk, M., Tozuka, T., Ishida, A., Yamagata, T., 2004. Can luzon strait transport play a role in conveying the impact of ENSO to the South China Sea? J. Clim. 17, 3644–3657. https://doi.org/10.1175/1520-0442(2004)017<3644:CLSTPA>2.0.CO;2.
Shaw, P.T., 1996. Winter upwelling off Luzon in the northeastern South China Sea. J. Geophys. Res. Oceans 101, 16435–16448. https://doi.org/10.1029/96JC01064.
Sheremet, V.A., 2001. Hysteresis of a western boundary current leaping across a gap. J. Phys. Oceanogr. 31, 1247–1259. https://doi.org/10.1175/1520-0485(2001)031<1247:HOAWBC>2.0.CO;2.
SSALTO/DUACS. (2011). User handbook: (M)SLA and (M)ADT near-real time and delayed time products. Cls_dos_nt_06-034 issue 2.5, archiving, validation and interpretation of satellite oceanographic data (AVISO) .
Sun, Z., et al., 2020. Three-dimensional structure and interannual variability of the Kuroshio Loop Current in the northeastern South China Sea. J. Phys. Oceanogr. 50 (9), 2437–2455. https://doi.org/10.1175/JPO-D-20-0058.1.
Sun, Z., Zhang, Z., Zhao, W., Tian, J., 2016. Interannual modulation of eddy kinetic energy in the northeastern South China Sea. J. Geophys. Res. Oceans 121, 3190–3201. https://doi.org/10.1002/2015JC011497.
Tozuka, T., Qu, T., Yamagata, T., 2015. Impacts of South China Sea throughflow on the mean state and El Nino/Southern Oscillation as revealed by a coupled GCM. J. Oceanogr. 71 (1), 105–114. https://doi.org/10.1007/s10872-014-0265-1.
Wang, J., Chern, C.-S., 1987. The warm-core eddy in the northern South China Sea. I. Preliminary observations on the warm-core eddy (in Chinese with English abstract). Acta Oceanogr Taiwanic 18, 92–103.
Wang, G., Su, J., Chu, P., 2003. Mesoscale eddies in the South China Sea observed with altimeter data. Geophys. Res. Lett. 30 (21), 2121. https://doi.org/10.1029/2003GL018532.
Wang, H., Wang, D., Liu, G., Wu, H., Li, M., 2012. Seasonal variation of eddy kinetic energy in the South China Sea. Acta Oceanol. Sin. 66 (1), 85–94. https://doi.org/10.1007/s13131-012-0170-7.
Wu, C.-R., Chiang, T.-L., 2007. Mesoscale eddies in the northern South China Sea. Deep-Sea Res. II 54, 1575–1588. https://doi.org/10.1016/j.dsr2.2007.05.008.
Wu, B., Gan, J., 2023. Seasonal modulation of the eddy kinetic energy and subtropical countercurrent near the western North Pacific boundary. J. Geophys. Res. Oceans 128. https://doi.org/10.1029/2022JC019160 e2022JC019160.
Wu, B., Lin, X., Yu, L., 2020a. Decadal to Multidecadal Variability of the Mixed Layer to the South of Kuroshio Extension region. J. Clim. 33 (17), 7697–7714. https://doi.org/10.1175/JCLI-D-20-0115.1.
Wu, B., Lin, X., Yu, L., 2020b. North Pacific Subtropical Mode Water Controlled by the Atlantic Multi-Decadal Variability. Nat. Clim. Chang. 10, 238–243. https://doi.org/10.1038/s41558-020-0692-5.
Wu, B., Xu, L., Lin, X., 2022. Decadal to Multidecadal variability of the Western North Pacific Subtropical Front and Countercurrent. J. Geophys. Res. Oceans 127 (2). https://doi.org/10.1029/2021JC018059 e2021JC018059.
Wu, B., Gan, J., Lin, X., Qiu, B., 2024. Long-term Decreasing of Sea Level along Latitude of the Luzon Strait during 1993–2020: Surface versus Subsurface Perspectives. J. Geophys. Res. Oceans 129. https://doi.org/10.1029/2023JC019805 e2023JC019805.
Wu, C.-R., Wang, Y.-L., Lin, Y.-F., Chiang, T.-L., Wu, C.-C., 2016. Weakening of the Kuroshio intrusion into the South China Sea under the global warming hiatus. *IEEE J. Sel. Top. Appl. Earth Obs. Remote Sens.* 9, 5064–5070. https://doi.org/10.1109/JSTARS.2016.2574941.
Wu, C.R., Wang, Y.L., Lin, Y.F., Chao, S., 2017. Intrusion of the Kuroshio into the South and East China Seas. Sci. Rep. 7, 7895. https://doi.org/10.1038/s41598-017-08206-4.
Wu, B., Xu, L., 2023. Zonally Asymmetric Multidecadal Variability of the North Pacific Subtropical Fronts. J. Clim. 36 (9), 2833–2846. https://doi.org/10.1175/JCLI-D-22-0299.1.
Xue, H., Chai, F., Pettigrew, N.R., Xu, D., Shi, M., Xu, J., 2004. Kuroshio intrusion and the circulation in the South China Sea. J. Geophys. Res. 109, C02017. https://doi.org/10.1029/2002JC001724.
Yang, H., Liu, Q., 2003. Forced Rossby wave in the northern South China Sea. Deep Sea Res. Part I 50, 917–926. https://doi.org/10.1016/S0967-0637(03)00074-8.
Yang, H., Wu, L., Liu, H., Yu, Y., 2013. Eddy energy sources and sinks in the South China Sea. J. Geophys. Res. Oceans 118, 4716–4726. https://doi.org/10.1002/jgrc.20343.
Yuan, D., Song, X., Yang, Y., Dewar, W.K., 2019. Dynamics of mesoscale eddies interacting with a western boundary current flowing by a gap. J. Geophys. Res. Oceans 124, 4117–4132. https://doi.org/10.1029/2019JC014949.
Yuan, D., Wang, Z., 2011. Hysteresis and dynamics of a western boundary current flowing by a gap forced by impingement of mesoscale eddies. J. Phys. Oceanogr. 41, 878–888. https://doi.org/10.1175/2010JPO4489.1.
Zhang, Y., Zhang, Z., Chen, D., Qiu, B., Wang, W., 2020. Strengthening of the Kuroshio current by intensifying tropical cyclones. Science 368, 988–993. https://doi.org/10.1126/science.aax5758.
Zhang, Z., Zhao, W., Tian, J., Liang, X., 2013. A mesoscale eddy pair southwest of Taiwan and its influence on deep circulation. J. Geophys. Res. Oceans 118, 6479–6494. https://doi.org/10.1002/2013JC008994.
Zhang, Z., Zhao, W., Tian, J., Yang, Q., Qu, T., 2015. Spatial structure and temporal variability of the zonal flow in the Luzon Strait. J. Geophys. Res. Oceans 120, 759–776. https://doi.org/10.1002/2014JC010308.
Zhang, Z., Tian, J., Qiu, B., Zhao, W., Chang, P., Wu, D., Wan, X., 2016. Observed 3D structure, generation, and dissipation of oceanic mesoscale eddies in the South China Sea. Sci. Rep. 6 (24), 349. https://doi.org/10.1038/srep24349.
Zhang, Z., Zhao, W., Qiu, B., Tian, J., 2017. Anticyclonic eddy sheddings from Kuroshio loop and the accompanying cyclonic eddy in the northeastern South China Sea. J. Phys. Oceanogr. 47 (6), 1243–1259. https://doi.org/10.1175/jpo-d-16-0185.1.
Zhao, Y., Yang, Y., Liang, X.S., Zhang, Y., 2022. Different mechanisms for the seasonal variations of the mesoscale eddy energy in the South China Sea. Deep Sea Res. Part I 179, 103677. https://doi.org/10.1016/j.dsr.2021.103677.
Zheng, Q., Tai, C., Hu, J., Lin, H., Zhang, R., Su, F., Yang, X., 2011. Satellite altimeter observations of nonlinear Rossby eddy-Kuroshio interaction at the Luzon Strait. J. Oceanogr. 67, 365–376. https://doi.org/10.1007/s10872-011-0035-2.
Zheng, Q., Xie, L., Zheng, Z., Hu, J., 2017. Progress in research of mesoscale eddies in the South China Sea. Advances in Marine Science (in Chinese) 35 (2), 131–158.
Zhou, S., Huang, P., Wang, L., Hu, K., Huang, G., Hu, P., 2024. Robust changes in global subtropical circulation under greenhouse warming. Nat. Commun. 15, 96. https://doi.org/10.1038/s41467-023-44244-5.
Zhu, Y., Yao, J., Xu, T., Li, S., Wang, Y., Wei, Z., 2022. Weakening trend of Luzon Strait overflow transport in the past two decades. Geophys. Res. Lett. 49. https://doi.org/10.1029/2021GL097395 e2021GL097395.
Zu, T., Wang, D., Yan, C., Belkin, I., Zhuang, W., Chen, J., 2013. Evolution of an anticyclonic eddy southwest of Taiwan. Ocean Dyn. 63, 519–531. https://doi.org/10.1007/s10236-013-0612-6.